# Bench-Top Cooling of a Microwave Mode Using an Optically Pumped Spin Refrigerator

Hao Wu, Shamil Mirkhanov, Wern Ng, and Mark Oxborrow*

*Department of Materials, Imperial College London, Exhibition Road, London SW7 2AZ, United Kingdom*

(Received 31 March 2021; accepted 4 June 2021; published 29 July 2021)

We experimentally demonstrate the temporary removal of thermal photons from a microwave mode at 1.45 GHz through its interaction with the spin-polarized triplet states of photo-excited pentacene molecules doped within a $p$-terphenyl crystal at room temperature. The crystal functions electromagnetically as a narrowband cryogenic load, removing photons from the otherwise room-temperature mode via stimulated absorption. The noise temperature of the microwave mode dropped to $50^{+18}_{-32}$ K (as directly inferred by noise-power measurements), while the metal walls of the cavity enclosing the mode remained at room temperature. Simulations based on the same system's behavior as a maser (which could be characterized more accurately) indicate the possibility of the mode's temperature sinking to ~10 K (corresponding to ~140 microwave photons). These observations, when combined with engineering improvements to deepen the cooling, identify the system as a narrowband yet extremely convenient platform—free of cryogenics, vacuum chambers, and strong magnets—for realizing low-noise detectors, quantum memory, and quantum-enhanced machines (such as heat engines) based on strong spin-photon coupling and entanglement at microwave frequencies.

DOI: 10.1103/PhysRevLett.127.053604

On a warm planet, electromagnetic noise associated with thermal (blackbody) radiation is the ubiquitous bugbear of quantum measurements [1]—especially at microwave frequencies, where a quantum of energy pales in comparison with $k_B T$. In a single electromagnetic mode of frequency $f_{\mathrm{mode}}$, the mean occupation number of thermal photons is $\bar{n} = [\exp(h f_{\mathrm{mode}}/k_B T) - 1]^{-1}$, equating to ~6200 for a microwave mode at 1 GHz at room temperature. These photons show up as noise on any signal extracted from the mode via a coupler and can limit the speed at which an EPR or NMR spectrum or MRI scan is taken. It is thus extremely challenging to attain the single-photon limit at microwave (or lower) frequencies with sources [2–4], sensors [5,6], and/or detectors [7,8] as is necessary to implement quantum Hanbury-Brown and Twiss interferometry [9,10] or other more complex protocols exploiting entanglement.

The most familiar way of removing thermal photons and their associated noise is to cool the microwave circuitry down to cryogenic temperatures by housing it inside a dilution refrigerator. Such refrigerators, however, are bulky, mechanically fragile, and energy-guzzling (dissipating typically kilowatts during operation); these attributes alas exclude many applications. The alternative pursued here is similar to the use, in radiometry, of a cryogenic load connected (to the rest of the microwave circuitry) through a low-loss waveguide [11]. Albeit only possible over a narrow band of frequencies, the cryogenic load is here replaced by a room-temperature yet "spin-cold" quantum system capable of absorbing photons through stimulated absorption [2]. Mode cooling is only achieved within the linewidth of the exploited quantum transition, but this cooling still enables useful applications. Our method, which exploits a cavity of a high magnetic Purcell factor [12], is thus similar in spirit to recent, cryogenic implementations of radiative cooling [13,14] but where the cold reservoir is a spin bath.

Several decades ago, it was demonstrated that Rydberg atoms could remove thermal photons from millimeter-wave cavities (operating at ~100 GHz or higher) via stimulated absorption [15–21]. The vacuum equipment needed to do this was still quite bulky, however. Compared to our work at 1.45 GHz, presented here, the cavity modes cooled enjoyed a "head start" by containing far fewer thermal photons ($\bar{n} < 50$ at room temperature [20]) in the first place.

In this Letter, we demonstrate a compact refrigerator capable of operating at room temperature and pressure in zero applied magnetic field. It exploits pentacene molecules doped within a crystal of $p$-terphenyl that are spin-polarized through photoexcitation. The crystal with a doping concentration of 0.1% is placed in the bore of a dielectric ring made of crystalline strontium titanate (STO) [see Fig. 1(c)] housed within a cylindrical copper enclosure. The ring plus enclosure support a compact $\mathrm{TE}_{01\delta}$ microwave cavity mode whose lines of ac magnetic flux penetrate the crystal [see Fig. 1(b)], enabling effective photon ↔ spin coupling between the microwave mode and the pentacene molecules.

The lowest photoexcited triplet state of pentacene in $p$-terphenyl has been extensively investigated for its use in

 

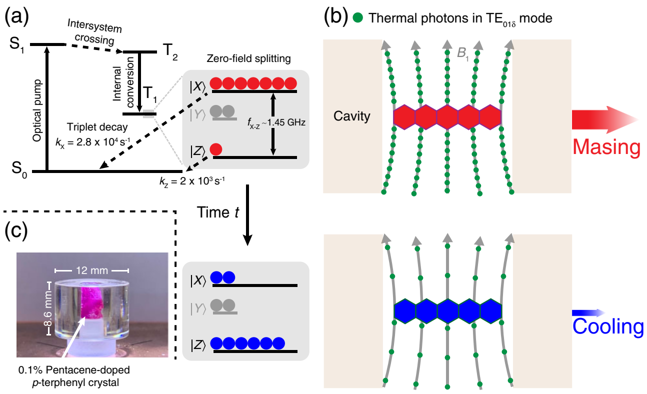


FIG. 1. (a) Simplified Jablonski diagram for molecular pentacene together with how the polarization across the $|X\rangle$ and $|Z\rangle$ sublevels of the lowest triplet state evolves from emissive (red circles) to absorptive (blue circles). (b) Dependence of the number of thermal photons (green dots) occupying the cavity's $TE_{01\delta}$ mode (gray lines of ac magnetic flux) on the population distribution across the $X-Z$ transition. (c) Photograph of the strontium titanate ring holding a 0.1% pentacene-doped $p$-terphenyl crystal. Its surrounding cylindrical copper enclosure is not shown.

dynamic nuclear polarization [22], room-temperature masers [12,23–26], quantum memory [27], and photovoltaics [28]. These previous studies have focused on pentacene's spin polarization immediately after photoexcitation. We instead exploit its opposite polarization at later times for the express purpose of mode cooling. Figure 1(a) shows how the triplet state is generated: a pentacene molecule is first excited from its singlet ground state ($S_0$) to its first excited singlet state ($S_1$). Then, through intersystem crossing, it transfers to its first excited triplet state ($T_2$) [29] and thereupon undergoes rapid internal conversion down to the lowest triplet state ($T_1$) while preserving its intersystem-crossing-acquired spin polarization. In zero applied magnetic field, $T_1$ comprises three separated sublevels: $|X\rangle$, $|Y\rangle$, and $|Z\rangle$, with initial populations 0.76:0.16:0.08 [30]. Initially, due to the sizable population inversion between the $|X\rangle$ and $|Z\rangle$ sublevels, thermal photons already occupying the cavity mode are multiplied up through stimulated emission across the $X-Z$ transition, resulting in maser oscillation [see the upper half of Fig. 1(b)]. Because the decay rate of $|Z\rangle$ ($2\times10^3\ \mathrm{s}^{-1}$) is considerably slower than that of $|X\rangle$ ($2.8\times10^4\ \mathrm{s}^{-1}$) and the spin-lattice relaxation between them is slow compared to these rates [31], the $|Z\rangle$ sublevel becomes, after masing has ceased, significantly overpopulated relative to $|X\rangle$ [see the bottom of Fig. 1(a)]. An extremely spin-cold two-level system across $|X\rangle \leftrightarrow |Z\rangle$ is thus temporarily formed. As shown conceptually in the lower half of Fig. 1(b), this system will act to *a*ttenuate (i.e., remove photons from) the electromagnetic mode through stimulated *a*bsorption. Mimicking Gordon and Townes' original acronym, we refer to this refrigeration process as "m*a*s*a*r" cooling.

To verify the concept, we first quantified the achievable spin temperature, $T_{X-Z}$, of the system using zero-field time-resolved EPR (TR-EPR) performed at room temperature, with the pentacene-doped $p$-terphenyl crystal pumped by a long-pulse dye laser. Details of this technique and how our crystal was grown have been reported elsewhere [31]. Here, the spin temperature is determined by the relative instantaneous populations of the $|X\rangle$ and $|Z\rangle$ sublevels [2]:

$$T_{X-Z} = hf_{X-Z}/[2k_B \tanh^{-1}(\Delta N/N)], \qquad (1)$$

where $f_{X-Z} = 1.4495$ GHz is the frequency of the $X-Z$ transition (at zero applied magnetic field), the population difference $\Delta N = N_Z - N_X$, and the total population $N = N_Z + N_X$.

Figure 2(a) displays the time profile of a typical 590-nm pump pulse, with the dye laser set to a low output such that no masing occurs; it lasts $\sim$300 $\mu$s and integrates to 250 mJ in energy. As displayed in Fig. 2(b), the measured signal, proportional to $\Delta N$, is strongly emissive for the first 250 $\mu$s but then becomes strongly absorptive for the next 500 $\mu$s. This dramatic crossover behavior, as was remarked on almost four decades ago [30], is well fitted by the model reported in Ref. [31]. Using it, the time profile of $N$ can be accurately simulated, as shown in Fig. 2(b). By substituting the simulated values of $\Delta N$ and $N$ into Eq. (1), one calculates that the maximum excursions of the polarization in the emissive and absorptive epochs correspond to Boltzmann-equivalent spin temperatures of $-170$ mK (red star) and 80 mK (blue triangle), respectively.

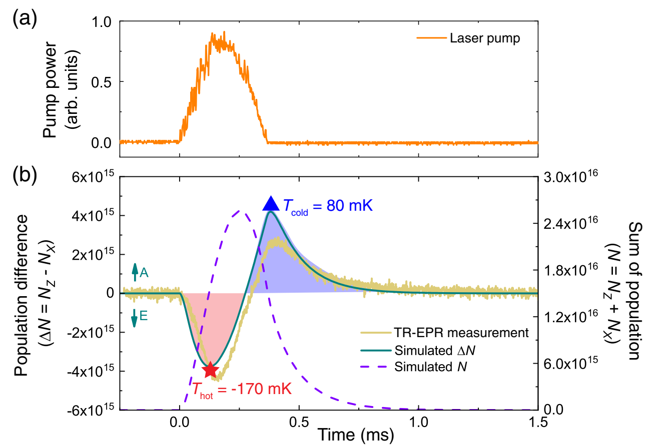


FIG. 2. (a) Instantaneous pump power of dye laser as used for our TR-EPR experiment. (b) Measured (olive green trace) and simulated (solid teal green line) TR-EPR response of a 0.1% pentacene-doped $p$-terphenyl crystal pumped by the same dye laser. This response measures the population difference ($\Delta N$) between the triplet sublevels $|X\rangle$ and $|Z\rangle$. The total population ($N$) in the two sublevels is modeled as a function of time and indicated by a dashed purple line. Red and blue shading emphasizes the emissive ($E$) and subsequently absorptive ($A$) epochs of the $X-Z$ transition, respectively.

We have probed the extent to which the coldness of the $X - Z$ transition can, in practice, be transferred to a target microwave mode by measuring the instantaneous power extracted from the mode by a metal loop threaded by a small fraction of the mode's ac magnetic flux. The power so extracted from this coupling "port" scales with the number of photons occupying the mode. The port's reflection coefficient, $\Gamma_c^0$, was adjusted (by changing the loop's size and insertion depth) to zero (critical coupling) in the absence of pumping. Our exact experimental setup, incorporating a high-gain heterodyne receiver, is shown in Fig. 1(c) and Fig. 3; our Supplemental Material provides additional technical details covering how the noise flow is modeled and calibrated [32]. At $f_{X-Z}$, the $TE_{01\delta}$ mode of our STO-loaded cavity had a measured linewidth at critical coupling of 400 kHz, inside of which the receiver's own measurement bandwidth of 50 kHz lay [see Fig. 3(b)].

Our principal results are shown in Fig. 4. The baseline at 0 dB in Fig. 4(a) includes both amplified noise received from the nonpumped cavity and the heterodyne receiver's self-generated noise. Excursions in the cavity's output power above this level reflect masing action; note, though,

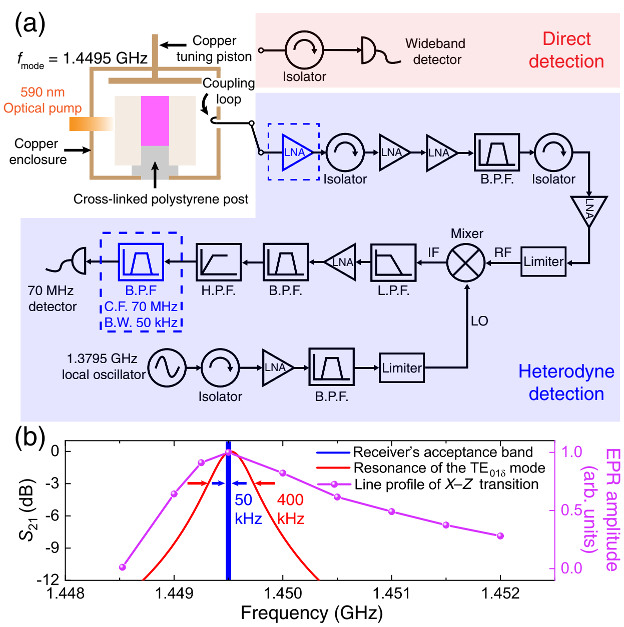


FIG. 3. (a) Experimental arrangement for measuring the energy of the $TE_{01\delta}$ mode of an STO cavity at room temperature. (Top left) STO ring (beige) housing a 0.1% pentacene-doped $p$-terphenyl crystal (pink) inside a copper enclosure (with hole for optical access). (Top right) Direct detection of the maser output with a wideband detector. (Bottom right) Heterodyne receiver suitable for measuring low mode energies. CF stands for center frequency; B.P.F., H.P.F., and L.P.F. stand for band-, high-, and low-pass filter, respectively. (b) Comparison between the receiver's acceptance band (blue) and the measured widths of the $TE_{01\delta}$ mode (red) and pentacene's $X - Z$ transition (purple).

that in Fig. 4(a) the peaks of the blue trace are compressed due to saturation of the later-stage amplifiers (and a protective diode limiter) in the heterodyne receiver. Dips below it arise from a reduction in the noise power of the microwave mode, reflecting masar cooling. Here, it is crucial to avoid mistaking the fool's gold of a "deep fade" (analogous to Rician fading, which will spontaneously occur at random times when observing narrowband noise) from genuine cause-and-effect cooling. We suppress deep fades by averaging the recorded instantaneous power over 11 separate (statistically independent) measurements performed in quick succession; the resultant average, shown in dark blue in Fig. 4(a), more faithfully indicates the cooling response.

Figure 4(a) shows that, during masing, deep notches in the outcoupled power are detected by the heterodyne receiver. We interpret them not as cooling but instead as being caused by collective coupling between the polarized pentacene spins (regarding the $X - Z$ transition as a two-level system) and the $TE_{01\delta}$ mode's microwave photons, causing the mode to split [27]. Temporarily, this splitting in frequency space is sufficient for the two arms of the spin-photon polariton to straddle the receiver's channel bandwidth (50 kHz), rendering them silent. Confronted by this phenomenon, the limited dynamical range (80 dB) and bandwidth of our receiver drove us to measure the outcoupled power directly with a separate wide bandwidth log detector, shown in Fig. 3; this allowed the $TE_{01\delta}$ mode's energy to be monitored accurately during periods of strong maser bursts; traces from this detector are shown in Figs. 4(d) and 4(e). The discernible Rabi oscillations in the three bursts have time-dependent frequencies ranging from 100 to 500 kHz because the number of pentacene spins available to interact with the microwave photons varies in response to the optical pump's time profile convolved with pentacene's own spin dynamics (see the Supplemental Material for details [32]). Oscillations faster than 500 kHz in the maser burst "I" are not resolved due to coarse sampling (owing to the limited memory depth of the oscilloscope used). Nevertheless, these traces show that the splitting of the $TE_{01\delta}$ mode can certainly exceed 100 kHz, beyond the 50-kHz bandwidth of our heterodyne receiver's bandpass filter.

Cooling of the microwave mode is demonstrated by the received noise power dipping below its ambient (room-temperature) level after each maser burst, i.e., the cooling epochs $A$ to $C$ shown in Fig. 4(a). The maximum reduction in noise power was found to be $\Delta P = -7.1^{+0.7}_{-0.9}$ dB by fitting, and we here invoke a noise model based on the "wave approach" [2,33] (see the Supplemental Material for the error and noise analysis [32]). Through this model, the relation between the mode's noise temperature (thus average photon population), $T_{\mathrm{mode}}$, and the reduction in noise power measured at the heterodyne receiver's output $\Delta P$ can be accurately calibrated; the curve is drawn in

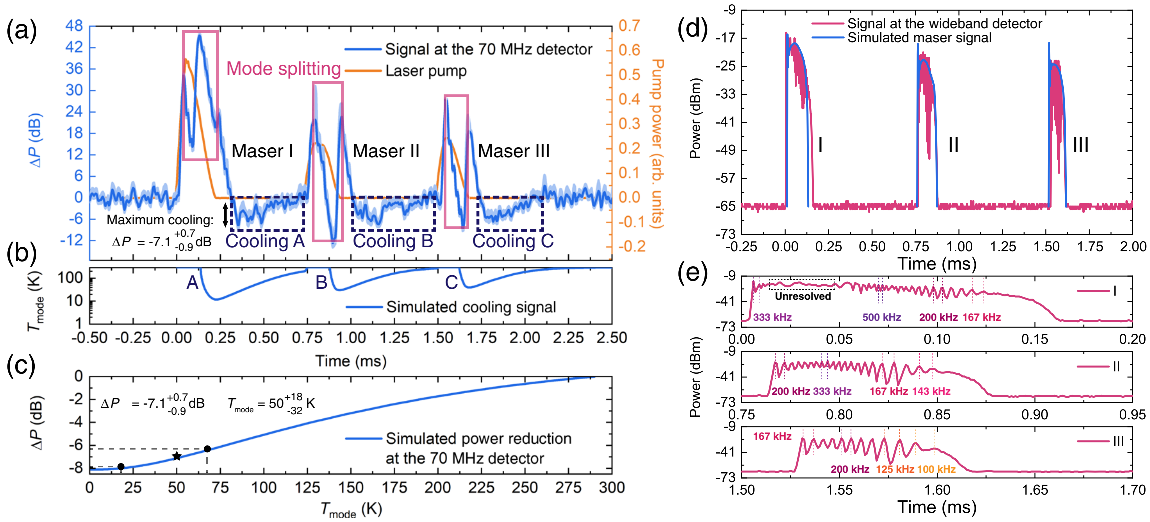


FIG. 4. (a) Instantaneous power outcoupled from microwave cavity in response to a train of three optical (590 nm) pump pulses as recorded by the heterodyne receiver. The average of 11 consecutive measurements is drawn in dark blue; the standard error associated with this average is displayed as the light blue region. Masing ($\Delta P > 0$) and cooling ($\Delta P < 0$) signals are labeled. The average instantaneous optical pump power is shown in orange. (b) Simulated noise temperature of the $TE_{01\delta}$ mode as a function of time. The bright masing regime is omitted. Note that delay in the receiver's SAW filter causes the experimental traces in (a) to be delayed (by $\sim$150 $\mu$s) relative to those shown here. (c) Simulated power reduction ($\Delta P$) at the receiver as a function of the noise temperature of the mode $T_{\text{mode}}$. The maximum power reduction observed in (a) and its associated $T_{\text{mode}}$ (black star); 95% upper and lower confidence limits are labeled (black circles). (d) Single trace (red) of the instantaneous outcoupled power of maser oscillation measured via direct detection with the wideband log detector. The simulated maser signals (blue) were obtained using the same model developed for simulating the cooling signals in (b). The pump source is the same as used in (a). (e) Enlargement of the three maser bursts in (a) with the time-dependent Rabi frequencies labeled.

Fig. 4(c). As shown in Fig. 4(a), the maximum reduction in noise power observed (occurring after the first maser burst) indicates that $T_{\text{mode}}$ drops from room temperature $T_0 = 290$ K to $50^{+18}_{-32}$ K. This degree of cooling comes close to the limits of our room-temperature instrumentation, primarily dictated by the input noise of the heterodyne receiver's first low-noise amplifier. A dip in the noise power corresponding to $T_{\text{mode}} \leq 12.5$ K cannot be discerned above the receiver's noise floor at $-8.1$ dB.

The evolution of $T_{\text{mode}}$ can also be estimated, via modeling, from the instantaneous outcoupled power as measured by the wideband detector [top of Fig. 3(a)], whose signal faithfully reflects the number of photons $q(t)$ as a function of time $t$ in the cavity during each maser burst [see Fig. 4(d)]. We point out that, similar to the heterodyne detection of extremely weak maser bursts from Rydberg atoms [34], the measured maser signals [shown in Fig. 4(a)] from our receiver suffer both temporal delay and spread on account of its narrowest bandpass (SAW) filter. The actual duration of the maser bursts is indicated in Figs. 4(d) and 4(e), where the longest burst lasts about 160 $\mu$s. The required modeling involves solving semi-classical rate equations (see the Supplemental Material [32]). This approach cannot simulate the Rabi oscillations observed experimentally during epochs of masing but can accurately predict the power envelope of each maser burst [see Fig. 4(d)]. Using the same values of fitted parameters, the same model can be used to predict the population dynamics and hence the photon number $q(t)$ during each cooling epoch [see Fig. 4(b)]. To accomplish this, the relationships $q = [\exp(hf_{\text{mode}}/k_B T_{\text{mode}}) - 1]^{-1}$ and $P_{\text{maser}} = qhf_{\text{mode}}\kappa_c k/(1+k)$ [27] are used; $P_{\text{maser}}$ is the outcoupled maser power shown in Fig. 4(d), $\kappa_c = 2\pi \times 0.4$ MHz is the cavity decay rate (corresponding to the cavity decay time $\sim$400 ns), and $k$ is the coupling coefficient of the cavity's port.

Figure 4(b) implies the cooling effect occurs almost immediately after the cessation of maser oscillation, when $|Z\rangle$ becomes overpopulated and the rate of stimulated absorption from $|Z\rangle$ to $|X\rangle$ exceeds the rates of cavity decay (i.e., the rate at which thermal photons fill up the cavity) and spin-lattice relaxation. The duration of cooling ($\sim$625 $\mu$s) is limited by the need to satisfy $N_Z > N_X$, which is controlled by the lifetime of $|Z\rangle$ ($\tau_Z \sim 500$ $\mu$s) relative to that of $|X\rangle$, the former being 1 order of magnitude longer [31]. The depth of the cooling depends on the rate of stimulated absorption, which is proportional to the population difference (equal to $N_Z - N_X$) between $|X\rangle$ and $|Z\rangle$, and follows its own time evolution (see the Supplemental Material [32]). According to our simulation, the lowest $T_{\text{mode}}$ reached was around 10 K, corresponding to $\sim$140 photons in the microwave mode. This is close to the lower 95% confidence limit of $T_{\text{mode}}$ (i.e., $50^{+18}_{-32}$ K) inferred from our calibration curve relating $\Delta P$ to $T_{\text{mode}}$.

In conclusion, our work demonstrates that the photoexcited triplet state of pentacene doped in $p$-terphenyl can be exploited to realize a spin refrigerator that cools, by the stimulated absorption of thermal photons, an electromagnetic mode of a microwave cavity from room temperature down to a few tens of kelvin (if not lower). The cooling performance can certainly be improved upon through engineering, e.g., increasing the crystal's magnetic filling factor, and through material science, i.e., identifying (then growing) crystals exhibiting greater absorptive spin polarization. The approach reported here opens up a new benchtop, room-temperature route to investigating quantum entanglement [46] and to the realization of quantum heat engines [47,48]. A cold cavity mode so prepared could be exploited to boost measurement sensitivity in (pulsed) EPR and NMR experiments [49], radiatively cool a secondary system [13,14], or reduce errors in quantum gate operations [50].

We thank Ben Gaskell of Gaskell Quartz Ltd (London) for making the strontium titanate ring used. This work was supported by the U.K. Engineering and Physical Sciences Research Council through Grants No. EP/K037390/1 and No. EP/M020398/1. H. W. acknowledges financial support from the China Scholarship Council (CSC) and the Imperial College London for a CSC-Imperial Ph.D. scholarship.

*Corresponding author.
m.oxborrow@imperial.ac.uk

[1] Y. Shih, *An Introduction to Quantum Optics: Photon and Biphoton Physics* (CRC Press, London, 2011).
[2] A. E. Siegman, *Microwave Solid-State Masers* (McGraw-Hill, New York, 1964).
[3] K. Benmessai, D. L. Creedon, M. E. Tobar, P.-Y. Bourgeois, Y. Kersalé, and V. Giordano, Phys. Rev. Lett. **100**, 233901 (2008).
[4] J. P. Gordon, H. J. Zeiger, and C. H. Townes, Phys. Rev. **99**, 1264 (1955).
[5] P. Meystre, Ann. Phys. (Berlin) **525**, 215 (2013).
[6] K. C. Cox, D. H. Meyer, F. K. Fatemi, and P. D. Kunz, Phys. Rev. Lett. **121**, 110502 (2018).
[7] K. Inomata, Z. Lin, K. Koshino, W. D. Oliver, J.-S. Tsai, T. Yamamoto, and Y. Nakamura, Nat. Commun. **7**, 12303 (2016).
[8] J. Wrachtrup and A. Finkler, J. Magn. Reson. **269**, 225 (2016).
[9] R. Hanbury-Brown and R. Q. Twiss, Nature (London) **177**, 27 (1956).
[10] E. Knill, R. Laflamme, and G. Milburn, Nature (London) **409**, 46 (2001).
[11] M. Gervasi, G. Bonelli, G. Sironi, C. F., A. Passerini, and S. Casani, Rev. Sci. Instrum. **66**, 4798 (1995).
[12] J. D. Breeze, K.-J. Tan, B. Richards, J. Sathian, M. Oxborrow, and N. M. Alford, Nat. Commun. **6**, 6215 (2015).
[13] B. Albanese, S. Probst, V. Ranjan, C. W. Zollitsch, M. Pechal, A. Wallraff, J. J. Morton, D. Vion, D. Esteve, E. Flurin *et al.*, Nat. Phys. **16**, 751 (2020).
[14] M. Xu, X. Han, C.-L. Zou, W. Fu, Y. Xu, C. Zhong, L. Jiang, and H. X. Tang, Phys. Rev. Lett. **124**, 033602 (2020).
[15] T. F. Gallagher and W. E. Cooke, Phys. Rev. Lett. **42**, 835 (1979).
[16] H. Figger, G. Leuchs, R. Straubinger, and H. Walther, Opt. Commun. **33**, 37 (1980).
[17] E. Beiting, G. Hildebrandt, F. Kellert, G. Foltz, K. Smith, F. Dunning, and R. Stebbings, J. Chem. Phys. **70**, 3551 (1979).
[18] P. Koch, H. Hieronymus, A. Van Raan, and W. Raith, Phys. Lett. **75A**, 273 (1980).
[19] W. P. Spencer, A. G. Vaidyanathan, D. Kleppner, and T. W. Ducas, Phys. Rev. A **25**, 380 (1982).
[20] J. M. Raimond, P. Goy, M. Gross, C. Fabre, and S. Haroche, Phys. Rev. Lett. **49**, 117 (1982).
[21] S. Haroche and J. Raimond, Adv. At. Mol. Phys. **20**, 347 (1985).
[22] M. Iinuma, Y. Takahashi, I. Shaké, M. Oda, A. Masaike, T. Yabuzaki, and H. M. Shimizu, Phys. Rev. Lett. **84**, 171 (2000).
[23] M. Oxborrow, J. D. Breeze, and N. M. Alford, Nature (London) **488**, 353 (2012).
[24] E. Salvadori, J. D. Breeze, K.-J. Tan, J. Sathian, B. Richards, M. W. Fung, G. Wolfowicz, M. Oxborrow, N. M. Alford, and C. W. Kay, Sci. Rep. **7**, 41836 (2017).
[25] H. Wu, S. Mirkhanov, W. Ng, K.-C. Chen, Y. Xiong, and M. Oxborrow, Opt. Express **28**, 29691 (2020).
[26] H. Wu, X. Xie, W. Ng, S. Mehanna, Y. Li, M. Attwood, and M. Oxborrow, Phys. Rev. Applied **14**, 064017 (2020).
[27] J. D. Breeze, E. Salvadori, J. Sathian, N. M. Alford, and C. W. Kay, npj Quantum Inf. **3**, 40 (2017).
[28] D. Lubert-Perquel, E. Salvadori, M. Dyson, P. N. Stavrinou, R. Montis, H. Nagashima, Y. Kobori, S. Heutz, and C. W. Kay, Nat. Commun. **9**, 4222 (2018).
[29] S. Bogatko, P. D. Haynes, J. Sathian, J. Wade, J.-S. Kim, K.-J. Tan, J. D. Breeze, E. Salvadori, A. Horsfield, and M. Oxborrow, J. Phys. Chem. C **120**, 8251 (2016).
[30] D. J. Sloop, H.-L. Yu, T.-S. Lin, and S. Weissman, J. Chem. Phys. **75**, 3746 (1981).
[31] H. Wu, W. Ng, S. Mirkhanov, A. Amirzhan, S. Nitnara, and M. Oxborrow, J. Phys. Chem. C **123**, 24275 (2019).
[32] See Supplemental Material, which includes Refs. [2,24,26,30,31,33–45], at http://link.aps.org/supplemental/10.1103/PhysRevLett.127.053604 for details of experimental method, model of pentacene's spin dynamics, and noise analysis.
[33] V. Đorđević, Z. Marinković, G. Crupi, O. Pronić-Rančić, V. Marković, and A. Caddemi, Int. J. Numer. Model. **30**, e2138 (2017).
[34] L. Moi, C. Fabre, P. Goy, M. Gross, S. Haroche, P. Encrenaz, G. Beaudin, and B. Lazareff, Opt. Commun. **33**, 47 (1980).
[35] M. Oxborrow, IEEE Trans. Microwave Theory Tech. **55**, 1209 (2007).
[36] M. Pollnau, T. Graf, J. E. Balmer, W. Lüthy, and H. P. Weber, Phys. Rev. A **49**, 3990 (1994).
[37] F. G. Patterson, H. W. H. Lee, W. L. Wilson, and M. D. Fayer, Chem. Phys. **84**, 51 (1984).
[38] K. Takeda, K. Takegoshi, and T. Terao, J. Chem. Phys. **117**, 4940 (2002).

[39] K. A. Nelson, D. R. Lutz, M. D. Fayer, and L. Madison, Phys. Rev. B **24**, 3261 (1981).
[40] F. W. Deeg, L. Madison, and M. Fayer, Chem. Phys. **94**, 265 (1985).
[41] T.-C. Yang, D. J. Sloop, S. Weissman, and T.-S. Lin, J. Chem. Phys. **113**, 11194 (2000).
[42] P. Penfield, IRE Transactions on Circuit Theory **9**, 84 (1962).
[43] PMA2-33LN+ datasheet and .s2p file, Mini-Circuits (2019).
[44] J. D. Kraus, *Radio Astronomy* (Cygnus-Quasar Books, Powell, OH, 1986).
[45] M. Oxborrow, Maser assembly, U.S. patent No. 9,608, 396 (2017).
[46] S. Haroche and J.-M. Raimond, *Exploring the Quantum: Atoms, Cavities, and Photons* (Oxford University Press, New York, 2006).
[47] H. E. Scovil and E. O. Schulz-DuBois, Phys. Rev. Lett. **2**, 262 (1959).
[48] J. Klatzow, J. N. Becker, P. M. Ledingham, C. Weinzetl, K. T. Kaczmarek, D. J. Saunders, J. Nunn, I. A. Walmsley, R. Uzdin, and E. Poem, Phys. Rev. Lett. **122**, 110601 (2019).
[49] J. C. Mollier, J. Hardin, and J. Uebersfeld, Rev. Sci. Instrum. **44**, 1763 (1973).
[50] K. Henschel, J. Majer, J. Schmiedmayer, and H. Ritsch, Phys. Rev. A **82**, 033810 (2010).